CHALMERS

Integration of a population balance equation into CFD modelling of high shear wet granulation

Master of Science Thesis within the Innovative and Sustainable Chemical Engineering program

SIMON LUNDEVALL

Department of Chemical and Biological Engineering
Division of Chemical Engineering
CHALMERS UNIVERSITY OF TECHNOLOGY
Göteborg, Sweden 2011

Integration of a population balance equation into CFD modelling of high shear wet granulation

Master of Science Thesis within the Innovative and Sustainable Chemical Engineering program

SIMON LUNDEVALL

SUPERVISOR:
Per Abrahamsson, Chalmers University of Technology

EXAMINER:
Anders Rasmuson, Chalmers University of Technology

Department of Chemical and Biological Engineering
Division of Chemical Engineering
CHALMERS UNIVERSITY OF TECHNOLOGY
Göteborg, Sweden, 2011

Integration of a population balance equation into CFD modeling of high shear wet granulation
Master of Science Thesis within the Innovative and Sustainable Chemical Engineering program
SIMON LUNDEVALL

Department of Chemical and Biological Engineering
Division of Chemical Engineering
Chalmers University of Technology
SE-412 96 Göteborg
Sweden
Telephone: +46 (0)31-772 1000

Chalmers University of Technology
Göteborg, Sweden 2011

Integration of a population balance equation into CFD modeling of high shear wet granulation
Master of Science Thesis within the *Innovative and Sustainable Chemical Engineering* program
SIMON LUNDEVALL
Department of Chemical and Biological Engineering
Division of Chemical Engineering
Chalmers University of Technology

ABSTRACT
Granulation is a commonly used process operation in the pharmaceutical industry when manufacturing tablets. In order to optimize the process and be able to predict industrial scale performance process models are needed. A population balance equation can be used to model a particle system if the mechanisms behind the changes of the population are known. A promising method for solving the population balance equation is the quadratic method of moments (QMOM), where the statistical moments of the population are modeled instead of solving the actual number distribution directly. This method is suited if a rough estimation of the population is sufficient rather than the exact solution. In fluid dynamic systems, computational fluid dynamics (CFD) is one powerful tool which can be used to describe three-dimensional flow fields. With information of local flow conditions it is possible to model the granulation mechanisms accounting for non-ideal mixing. The difficulties with this approach are to describe the mechanisms for aggregation and breakage and model the flow field for such dense particle systems where shear forces become large.

By investigating different aggregation kernels, possibilities and difficulties of the integration of population balance into the flow field solver using has been evaluated.

The granular temperature in the system does not have a major influence on the system. The number distribution does not have a development that physically correlates to the population balance equation.

It has been concluded that there is a big potential in the modeling of a population balance. Using the QMOM solver technique is not straight forward while the discrete method is computationally very demanding why the choice between a moment and a fractional based solver should be carefully considered.

Keywords: High shear granulation, population balance, quadrature method of moments, CFD, Euler-Euler, KTGF.

Table of Contents

1 Introduction

1.1 Background

Wet granulation in high shear mixing units is an important processing step when manufacturing tablets in the pharmaceutical industry. Granulation is an intermediate step in the tablet manufacturing process where granules are produced from a powder blending consisting of an active substance and filler. Typical fillers are microcrystalline cellulose (MCC) as well as lactose and calcium phosphate. The granules are then dried, milled and compressed into tablets. The main reasons why the tablets are produces from granules instead from powder directly are that the granules are much easier to handle since granulate shows a more flowable behavior compared to powder. Second, the homogeneity of the active substance is favored by the granulation. Also, the risk for dust explosion is decreased compared to when powders are handled.

For process control, optimizing and scale-up problems it is of great interest to have a good model in which all occurring physical mechanisms are described. The granulation process is a complex system to model in the sense that large ranges of volume fraction of particles are present and at the same time as particles properties changes due to liquid addition, aggregation and breakage.

The most common way to model a granulation process including many different particle sizes is through a population balance equation (PBE) (Scarlett, 2001). PBE is one approach of modeling which can be used to describe changes in any property of a population. In this work a one-dimensional PBE over the particle diameter is derived which results corresponds to the particle size distribution. In order to describe the mechanisms behind the changes in particle size such as aggregation and breakage, information about the process condition and the local flow field is needed.

Computational fluid dynamic (CFD) simulations can be used to investigate the dynamics of a fluid system where the Navier-Stokes equations are solved numerically. The Euler-Euler model, also called multi fluid model, is used to describe multi phase systems including very dense particle flows as granulation. This model treats the particles as a continuum which is a drawback of the physical description but gives an advantage in the computational load compared to other multiphase models. This makes it possible to simulate unit operations at industrial scale.

The model developed in this work is based on a population balance equation (PBE) coupled to the fluid dynamics in a granular system. The particle size dynamics cannot be modeled by the Euler-Euler model itself why a improvement in simulation accuracy can be achieved when the PBE is integrated.

1.2 Objective

The main objective of this thesis is to investigate the integration of ANSYS FLUENT: s population balance module into the Euler-Euler multiphase model in order to build a well physically described model of the granulation process. One part of the work aims to investigate the potential of estimating the PBE through its statistical moments. Also, the possibilities and limitations of existing agglomeration kernels in ANSYS FLUENT are investigated.

1.3 Method

A literature study of different numerical methods for solving the PBE is performed. Different models of agglomeration kernels are also studied.

A PBE model is built based on previous models found in the literature. The model is then coupled to a converged flow field of a laboratory scaled granulator. Simulations of the process are performed in the commercial software ANSYS FLUENT 13.0. Evaluation of used models will only be relative since there are no experimental data for validation.

2 High shear wet granulation

Granulation is a process where small particle with typical diameters of 10-100 µm are mixed with a binder liquid, collides and form aggregates with sizes up to 1 mm in diameter. The granulation process is common in the pharmaceutical industry and is usually performed batch wise in a granulator. There are several different types of granulators used in the industry such as drum granulators, fluidized beds and also high shear mixers. The high shear mixer granulator operates without baffles and with the impeller typically close to the bottom. There is also a chopper installed which is used to break larger aggregates. The aggregation of smaller particles and the breakage of larger will act for a homogenous particle size distribution which is desired. It is also of great interest that the active substance is equally distributed over the granules to avoid locally concentration deviations and thereby ensure that the right amount of active substance is compressed in each tablet.

The granulation can be regarded as a three step process. First, a dry mixing period, where the active substance and one or several fillers are mixed together until the particle blending is considered homogenous. The second step is the liquid addition period where a liquid binder is sprayed over the particles and the particles starts to aggregate. The third and last step is the wet massing period where no more liquid is added but the aggregation and breakage continue until the process is stopped.

2.1 Granule characterization and granulation mechanisms

The granules can be characterized based on the moisture content that is carried. During the liquid addition period the powder particle will start to aggregate due to the formation of liquid bridges. Thereafter liquid and other powder particles are successively added to the aggregate and as a result, properties such as porosity and liquid saturation will change which affects how likely the different granulation mechanisms are to occur.

Among all mechanisms involved in granulation there are nucleation, liquid and solid bridging, coalescence of granules and dry particles, coating, liquid transfer between granules and breakages of granules into smaller granules or into its nuclei elements. The main steps in the agglomeration process are present in figure 2.1.1.

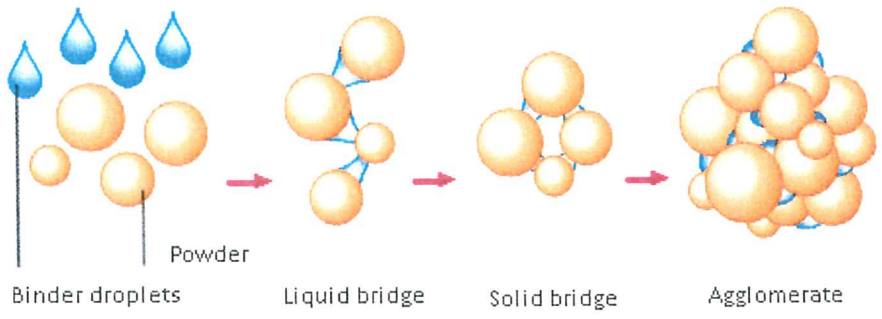

Figure 2.1.1 Typically mechanisms in the process of agglomeration (Glatt, 2011).

The different mechanisms are individually very difficult to model since kinetic expressions and rate constants are needed. For modeling, the process is normally described in three steps:

1. Nucleation, where dry powder particles first have contact with the liquid and form the smallest granule structure.
2. Coalescence, where two granules, or a granule and a powder particle aggregate.
3. Breakage, where granules break due to high shear forces.

In the literature of coalescence modeling, the mechanism is usually divided in two types of coalescence:

Type 1 Coalescence occurs when the kinetic energy is lost due to viscous dissipation in the binder liquid layer before the granule surfaces reach contact.

Type 2 Coalescence occurs after granule collision during rebound. Energy is lost not only by viscous dissipation but also by plastic deformation.

3 Computational fluid dynamics

Computational fluid dynamics is used in fluid dynamic systems in which three-dimensional models is necessary in order to account for non-ideal flow behavior. The purpose is to achieve more accurate physical models so that better predictions can be performed.

3.1 The governing transport equations

The motion of a fluid is described through a continuity equation which is the condition of mass conservation, and a momentum equation which relate the acceleration of a fluid element with the force acting on it. The continuity and the momentum equations can be written as

$$\frac{\partial \rho}{\partial t} + \nabla \cdot (\rho \vec{u}) = 0 \tag{3.1.1}$$

$$\frac{\partial}{\partial t}(\rho \vec{u}) + \nabla \cdot (\rho \vec{u}\vec{u}) = -\nabla P + \nabla \cdot \bar{\bar{\tau}} + \rho \vec{g} + \vec{F} \tag{3.1.2}$$

where ρ is the fluid density, $\vec{u}$ is the fluid velocity vector, P is pressure, $\bar{\bar{\tau}}$ is the viscous stress tensor, $\vec{g}$ is the gravitational acceleration and $\vec{F}$ is a source term representing all other external forces acting on the fluid element. Assuming the fluid is incompressible and has constant viscosity these equations can be simplified to the Navier-Stokes equations.

In order to solve these partial differential equations they have to be discretizied and solved numerically. This is done by dividing the geometry in small sub-volumes in which the equations can be solved as algebraic equations. In many problems it is sufficient with a steady state solution, otherwise the time as well as the physical space has to be discretizied and steady state solutions can be obtained while stepping forward in time.

4 Multiphase flow

In many fluid dynamic systems, the flow field is affected by a secondary phase such as a gaseous phase containing particles or droplets, or a liquid containing particles, droplets or bubbles. When the motion of a volume element consisting of multiple phases is to be described the governing equations has to be modified accordingly. There exist several different models for multiphase systems which all treat the discrete phase differently and they all have advantages for different applications. A classification of different flow situations can be used to determine what multiphase model is appropriate.

Multiphase flow fields are usually divided in separated flows and dispersed flows. If the secondary phase consists of particles, droplets or bubbles it is considered as dispersed. A dispersed flow can be considered either dense or dilute; this can be evaluated by the collision Stokes number which compares the time scale for the dispersed phase with the timescale of inter-particle interactions.

Whether the continuous phase interaction with the dispersed phase is significant or not can be evaluated with Stokes particle response number. This number is defined as the ratio between the time scale for the flow and the timescale for the discrete phase. If St >> 1 the discrete phase will be unaffected by surrounding flow and if St << 1the discrete phase will follow the flow completely.

The coupling between the phases can be summarized in three categories (Andersson et al., 2010). The first case is called one-way coupling and implies that the particles are affected by the continuous phase but do not affect the continuous phase. Second, is the case of two-way coupling where the two phases affect each other while the third case is identified as four-way coupling where not only the phases affect each other but also discrete inter-phase interactions occurs as for the case with particle collisions.

There are two different multiphase frameworks. At first, the Euler-Lagrangian, where the discrete phase is described by solving a momentum equation for each particle and couples the momentum changes to the continuous phase. This model is physically well described but becomes very computational expensive at larger discrete phase volume fractions since the Newton second law is to be derived for each discrete element and all possible collisions are considered. Second, the Euler-Euler method is used where all phases are treated as if they could be described as a continuum. This assumption leads to a set of unclosed equations which makes it necessary to introduce empirical relations in the model but in return it is possible to model very dense flows at industrial scale without exceeding the computational power available.

4.1 Eulerian-Eulerian framework

In the Euler-Euler model, particles are not described as a discrete phase but as a continuous medium with properties of a fluid. This raises a closure problem in the discrete phase momentum equation where a solid pressure and a solid viscosity are needed. In this section the Euler-Euler approach will be described and all the empirical expressions used for the closures are presented.

The mass and momentum transport equations are solved for each phase together with the condition that the sum of all phases volume fraction equals one.

$$\sum_k \alpha_k = 1 \tag{4.1.1}$$

For a solid-gas system there will be no mass transfer between the phases and with no source of mass or momentum the governing equations for the fluid phase are given as (Anderson and Jackson, 1967)

$$\frac{\partial}{\partial t}(\alpha_f \rho_f) + \nabla \cdot (\alpha_f \rho_f \vec{u}_f) = 0 \tag{4.1.2}$$

$$\frac{\partial}{\partial t}(\alpha_f \rho_f \vec{u}_f) + \nabla \cdot (\alpha_f \rho_f \vec{u}_f \vec{u}_f) = -\alpha_f \nabla P + \nabla \cdot (\alpha_f \bar{\bar{\tau}}_f) + \beta(\vec{u}_f - \vec{u}_s) + \alpha_f \rho_f \vec{g} \tag{4.1.3}$$

For the discrete phase the corresponding equations are written as:

$$\frac{\partial}{\partial t}(\alpha_s \rho_s) + \nabla \cdot (\alpha_s \rho_s \vec{u}_s) = 0 \tag{4.1.4}$$

$$\frac{\partial}{\partial t}(\alpha_s \rho_s \vec{u}_s) + \nabla \cdot (\alpha_s \rho_s \vec{u}_s \vec{u}_s) = -\alpha_s \nabla P - \nabla P_s + \nabla \cdot (\alpha_s \bar{\bar{\tau}}_s) - \beta(\vec{u}_f - \vec{u}_s) + \alpha_s \rho_s \vec{g} \tag{4.1.5}$$

In the equations above α_k is the volume fraction for phase k and β is a coefficient for momentum exchange between the phases. P_s is the discrete phase pressure; $\vec{g}$ is the acceleration due to gravity and $\bar{\bar{\tau}}$ is the viscous stress tensor associated with respective phase described by Newton's law of viscosity.

$$\bar{\bar{\tau}}_k = \mu_k\left(\nabla u_k + (\nabla u_k)^{\mathrm{T}}\right) + \left(\lambda_k - \frac{2}{3}\mu_k\right)(\nabla \cdot u_k)\bar{\bar{I}} \tag{4.1.6}$$

In the above stated equation, μ_k is the dynamic viscosity and λ_k is the bulk viscosity which accounts for granular compression and expansion resistance and is zero for a Newtonian fluid.

4.1.1 Interphase momentum exchange coefficient

The momentum exchange between the phases is limited to the drag force only since all other forces becomes negligible at higher granular volume fractions. The drag expression is typically based on the drag coefficient, C_D, which generally includes information of the particle shape and the local velocity differences between phases. For dense particle systems corrections are needed to take into account that the particles affect each other's drag. There exist several different expressions for the momentum exchange and the drag coefficient for dense systems in the literature. However, the expressions proposed by Wen and Yu (1966) have been used in this work.

$$\beta = \frac{3}{4} C_D \frac{\alpha_f \alpha_s \rho_f |u_f - u_s|}{d_s} \alpha_f^{-2.65} \tag{4.1.7}$$

$$C_D = \frac{24}{\alpha_f Re_p}\left[1 + 0.15(\alpha_f Re_p)^{0.687}\right] \tag{4.1.8}$$

The particle Reynolds number is defined as:

$$Re_p = \frac{d_s \rho_f |\vec{u}_f - \vec{u}_s|}{\mu_f} \tag{4.1.9}$$

4.1.2 Kinetic theory of granular flow

To close the momentum equation the kinetic theory of granular flow is applied. A detailed description of the theory is given by Gidaspow (1994). This theory is based on the kinetic theory of gases which describes properties of gases through averaging of the motion of molecules in the gas. When averaging the state of molecules, all information as location, speed and direction is lost for each individual molecule. Instead macroscopic properties as temperature and pressure are introduced to describe the state of the gas. Analogously with this theory, KTGF is used to describe averaged properties of a granular system.

In the KTGF the averaged fluctuating velocity of a particle is described by the introduced granular temperature, and is modeled through a transport equation. The following equation is proposed by Ding and Gidaspow (1990).

Granular temperature: $\Theta_s = \frac{1}{3}\overrightarrow{u'_s}^2$ (4.1.10)

$$\frac{3}{2}\left[\frac{\partial(\alpha_s\rho_s\Theta_s)}{\partial t} + \nabla\cdot(\alpha_s\rho_s\Theta_s\vec{u}_s)\right] = \left(-P_s\bar{\bar{I}} + \bar{\bar{\tau}}_s\right) : \nabla\vec{u}_s - \nabla\cdot(\kappa_\Theta\nabla\Theta) - \gamma_\Theta - \phi_\Theta \quad (4.1.11)$$

The left hand side terms represents accumulation and convection of granular temperature respectively. The right hand side terms represents generation, diffusion, dissipation and transfer of granular temperature between different granular phases. The equation can be simplified to an algebraic equation assuming a local steady state so that generation of granular temperature is balanced against dissipation. With this assumption equation (4.1.11) is reduced to equation 4.1.12.

$$0 = \left(-P_s\bar{\bar{I}} + \bar{\bar{\tau}}_s\right) : \nabla\vec{u}_s - \gamma_\Theta \quad (4.1.12)$$

The following expressions of granular temperature dissipation, solid pressure, granular bulk viscosity as well as the radial distribution function (equations 4.1.13 – 4.1.16) are all modeled as proposed by Lun et al. (1984).

$$\gamma_{\Theta_s} = \frac{12(1-e^2)g_0}{d_s\sqrt{\pi}}\rho_s\alpha_s^2\Theta_s^{3/2} \quad (4.1.13)$$

The solid pressure accounts for interactions between granules and consists of a kinetic part and a collision part where e is the normal coefficient of restitution which accounts for energy loss due to inelastic collisions.

$$P_s = \alpha_s\rho_s\Theta_s + 2g_0\alpha_s^2\rho_s\Theta_s(1+e) \quad (4.1.14)$$

Here g0 is the radial distribution function which is used as a correction of the collision probability as the granular phase becomes dense.

$$g_0 = \left[1 - \left(\frac{\alpha_s}{\alpha_{s,max}}\right)^{\frac{1}{3}}\right]^{-1} \quad (4.1.15)$$

The bulk viscosity, λ_k, accounts for granular compression and expansion resistance and is zero for a Newtonian fluid.

$$\lambda_s = \frac{4}{3}\alpha_s\rho_s d_s(1+e)\sqrt{\frac{\Theta_s}{\pi}} \quad (4.1.16)$$

The solid viscosity arises from momentum transfer by translation, collisions and also by friction between granules if the discrete phase is dense. The total solid viscosity is modeled as a sum of contributions from the different mechanisms.

$$\mu_s = \mu_{s,kinetic} + \mu_{s,collision} + \mu_{s,friction} \quad (4.1.17)$$

The expressions for the kinetic and collision part are both from Syamlal et al. (1993).

$$\mu_{s,kinetic} = \frac{\alpha_s\rho_s d_s\sqrt{\Theta_s\pi}}{6(3-e)}\left[1 + \frac{2}{5}(1+e)(3e-1)\alpha_s g_0\right] \quad (4.1.17)$$

$$\mu_{s,collision} = \frac{4}{5}\alpha_s^2\rho_s d_s(1+e)\sqrt{\frac{\Theta_s}{\pi}} \quad (4.1.18)$$

4.1.2.1 Frictional stress model

In very dense flow, particles will have long duration contact with each other which is not taken into account in the kinetic theory where collisions are assumed to be binary and instantaneous. So when such a dense flow exists with discrete phase volume fraction close to the granules maximum packing limit, the frictional part is needed in equation 4.1.17. The frictional viscosity is expressed by Schaeffer (1987) as a modification of Coulombs law

$$\mu_{s,friction} = \frac{P_f \sin\phi}{2\sqrt{I_{2D}}} \tag{4.1.19}$$

where φ is the angle of internal friction, I_{2D} is the second invariant of the strain rate tensor. P_f is the frictional part of the solid pressure which is modeled as proposed by Johnson and Jackson (1987)

$$P_f = Fr\frac{(\alpha_s - \alpha_{s,min})^n}{(\alpha_{s,max} - \alpha_s)^p} \tag{4.1.20}$$

where $\alpha_{s,min}$ is the critical volume fraction where the friction becomes important. $\alpha_{s,max}$ is the packing limit. Fr, n and p are all empirical constants.

5 Population balance theory

In this chapter the concept of population balances is described. The basis of how to model aggregation and how the equation can be solved is explained.

5.1 The general population balance equation

The general PBE is derived by choosing a set of internal coordinates and defining a number density function $n(\vec{x}, \emptyset, t)$ where $\vec{x} \in \Omega_{\vec{x}}$ and $\emptyset \in \Omega_{\emptyset}$ represents the external and internal coordinates respectively. The number density function represents the number of entities at a specific position with a specific set of properties according to $\vec{x}$ and $\emptyset$. The total number of entities in the system is obtained by integrating the number density function over the entire physical space as well as the internal coordinates.

$$\int_{\Omega_{\vec{x}}} \int_{\Omega_{\emptyset}} n(\vec{x}, \emptyset, t)\, d\emptyset d\vec{x} \tag{5.1.1}$$

A general PBE for the development of a volume based particle size distribution, n′, can be written as

$$\frac{\partial}{\partial t}[n'(V,t)] + \nabla \cdot [\vec{u} n'(V,t)] + \nabla_G \cdot [G_V n'(V,t)] = B_a - D_a + B_b - D_b \tag{5.1.2}$$

where the left hand side terms represents accumulation, convection and growth of particles for each particle size V. The right hand side terms represents birth and death of particles due to aggregation and breakage respectively. A review of the state of the art of the population balance limited to aggregation and breakage problems can be found in Ramkrishna (2000).

The PBE can also be expressed with a length based number density function so that particle length can be used as internal coordinate. When converting the volume based number density function into a length based it is necessary to know how the particle length relates to its volume. In this work the relation $V \propto L^3$ are considered. With this relation it follows that

$$n'(V,t)dV = n'(L^3,t)3L^2 dL = n(L,t)dL \tag{5.1.3}$$

where n(L, t) is the length based number density function. The length based PBE is then obtain if equation (5.2.1) is multiplied with $3L^2$.

When solving the PBE different numerical methods can be used. The first intuitive and straight forward way to solve the equation is the discrete population balance where the particle distribution is divided into discrete bins, a discretization of the PBE is found in Hounslow et al. (1988). This method has the major drawback that it is very computational expensive since a lot of bins may be required to reproduce the distribution which is concluded in Marchisio et al. (2003a). A very promising method which is used in this work is the quadrature method of moments (QMOM) first proposed by McGraw (1997) in a study of size-dependent growth of aerosols. QMOM is based on the standard method of moments used to describe particle formation and growth problems (Hulburt and Katz, 1964) where statistical moments of the distribution are modeled instead of the actual particle size distribution.

5.2 Quadrature method of moments

The statistical moments of the discrete phase properties which are used to reconstruct the number distribution function are defined as

$$m_k = \int_0^{\infty} n(L,t)\, L^k dL \tag{5.2.1}$$

which implies that the first moment of zero:th order represents the total number of particles in the system. If the particle diameter is modeled the first moments can be used to describe the physical properties of the populations as

$$N_{total} = m_0 \tag{5.2.2}$$

$$L_{total} = m_1 \tag{5.2.3}$$

$$A_{total} = m_2 K_a \tag{5.2.4}$$

$$V_{total} = m_3 K_v \tag{5.2.5}$$

where K_a and K_v are constants which relates area and volume of a particle to its characteristically length, for a sphere these constants equals π and $\pi/6$ respectively.

The QMOM proposed by McGraw (1997) applies a quadrature approximation of the moments as

$$m_k = \int_0^\infty n(L)\, L^k dL \approx \sum_{i=1}^{N} w_i\, L_i^k \tag{5.2.6}$$

where w_i and L_i are derived from the product-difference algorithm described by Gordon (1967). The essence of using the product-difference method is that w_i and L_i can be derived from lower order moments, it takes 2N moments to build an quadrature approximation of order N.

If the general transport equation 5.1.2 is limited to aggregation it can now be expressed in terms of moments as

$$\frac{\partial}{\partial t} m_k + \nabla \cdot (\vec{u} m_k) = \bar{B}_a - \bar{D}_a \tag{5.2.7}$$

where $\bar{B}_a$ and $\bar{D}_a$ represents the length based birth and death expression in terms of moment which can be found in Marchisio et al. (2003b).

The dynamic of the PBE is connected to the fluid dynamics through the Sauter mean diameter defined as

$$d_{32} = \frac{m_3}{m_2} \tag{5.2.8}$$

5.3 Aggregation

During the granulation process, particles collide with each other. Sometimes the particles will aggregate due to the collisions and sometimes they will not. The level of accessible liquid binder in the granules is qualitatively probably one of the most important parameters which influence the coalescence mechanism why the amount liquid binder is used to determine the probability whether two particles will aggregate or not.

The expressions for birth and death terms in the general PBE (eq. 5.1.2) are described by the rate of change of particles caused by aggregation.

$$B_a = \frac{1}{2}\int_0^V a(V - V', V')\, n'(V - V', t)\, n'(V', t)\, dV' \tag{5.3.1}$$

$$D_a = \int_0^\infty a(V, V')\, n'(V, t)\, n'(V', t)\, dV' \tag{5.3.2}$$

The factor 0.5 in the birth expression is to avoid counting collisions twice. These expressions and a derivation for the corresponding length based expression can be found in Marshisio et al. (2003b). The

aggregation kernel, a, describe how often particles will aggregate and can be expressed as a product of collision frequency and aggregation efficiency.

$$a_{i,j} = k_{i,j}\psi_{i,j} \tag{5.3.3}$$

5.3.1 Collision frequency

Two expressions for collision frequency, $k_{i,j}$, are investigated. First, the equipartition of kinetic energy (EKE) kernel has been evaluated and also one aggregation kernel based on the principals of KTGF.

The EKE kernel was first derived by Hounslow (1998) and is based on the kinetic theory of gases. It is assumed that the fluctuating kinetic energy is equally distributed between all particles. Also it is assumed that the local velocity of a granule is expressed using Reynold's decomposition $u_i = \bar{u}_i + u_i'$ where it is only the fluctuating part that depends on the granule size.

$$k_{i,j} = \beta_0(t)(d_i + d_j)^2\sqrt{\frac{1}{d_i^3} + \frac{1}{d_j^3}} \tag{5.3.4}$$

In the kernel expression d is the diameter of a particle and β_0 is a rate constant dependent on operation conditions and thus time.

The KTGF based aggregation kernel was derived by Rajniak et al. (2009). This kernel is based on a collision rate derived by Goldschmidt (2001). By neglecting gradients of mean particle velocities and assuming that all particles are of equal density the aggregation kernel can finally be expressed as

$$k_{i,j} = \hat{\beta}_0(t)g_0 d_{43}^{1,5}\sqrt{\frac{\pi\Theta}{2}}(d_i + d_j)^2\sqrt{\frac{1}{d_i^3} + \frac{1}{d_j^3}} \tag{5.3.5}$$

where Θ is the particles mean granular temperature, d_{43} is the ratio of the forth and third moment as an approximation of the mean particle diameter; $\hat{\beta}_0(t)$ is a rate constant dependent on process conditions.

5.3.2 Aggregation efficiency

Whether two colliding particles will successfully aggregate or not is dependent not only of the local flow condition, but also of the presence of binder liquid and the granule morphology. There exists empirical, semi-empirical and physical expressions for the aggregation efficiency, $\psi_{i,j}$. An overview of the different approaches can be found in Abberger (2007). The aggregation efficiency can be divided in a geometrical and a physical part (Stepanek et al., 2009). The geometrical part represents the probability for two particles to collide on a wet spot while the physical part describes whether the kinetic energy of impact is dissipated through the viscous layer during the time of the collision and through plastic deformation of the particles.

$$\psi_{i,j} = \psi_{i,j}^{geom}\psi_{i,j}^{phys} \tag{5.3.6}$$

$$\psi_{i,j}^{geom} = 1 - (1 - \eta_i)(1 - \eta_j) \tag{5.3.7}$$

In the geometrical part, η is the relative frequency of particles that collide at a region of accessible binder liquid defined in Stepanek et al. (2009) where a relation between accessible binder fraction and the composition of a granule (binder/solid ratio) was developed for different commonly used filler materials.

The physical part of the aggregation efficiency is based on the viscous Stokes number which is the ratio of impact kinetic energy to viscous dissipation in the liquid layer. Whether the viscous Stokes

number is smaller or larger than a critical value determines if aggregation is possible or not, this model was derived by Ennis et al. (1991) for non-deformable particles. Further analysis of the viscous Stokes number and its effect on the coalescence mechanism can be found in Liu et al. (2000) and Liu and Litster (2002) where the model was extended by accounting for energy dissipation due to plastic deformation. If energy loss due to plastic deformation is neglected which implies elastic collision for type 2 coalescence the physical criterion can be written as (Liu et al., 2000 and Liu and Litster, 2002)

$$\psi^{phys} = \begin{cases} 1 \; if \; St_v \leq ln\frac{\lambda}{h_a} \\ 0 \; if \; St_v > ln\frac{\lambda}{h_a} \end{cases} \qquad \textit{Type 1 coalescence} \tag{5.3.8}$$

$$\psi^{phys} = \begin{cases} 1 \; if \; St_v \leq 2ln\frac{\lambda}{h_a} \\ 0 \; if \; St_v > 2ln\frac{\lambda}{h_a} \end{cases} \qquad \textit{Type 2 coalescence} \tag{5.3.9}$$

$$St_v = \frac{8\tilde{m}u_0}{3\pi\mu\tilde{d}^2} \tag{5.3.10}$$

$$\tilde{m} = \frac{m_i m_j}{m_i + m_j} \tag{5.3.11}$$

$$\tilde{d} = \frac{d_i d_j}{d_i + d_j} \tag{5.3.12}$$

In the physical criterion λ is the liquid binder thickness and h_a is the surface roughness; μ is the binder viscosity and u_0 is the collision velocity.

The collision velocity is estimated by Gidaspow (1994) through the granular temperature as

$$u_0 = \frac{3}{2}\sqrt{\pi\Theta} \tag{5.3.13}$$

6 Granulation process model

6.1 Geometry

A laboratory scaled granulator is simulated in the software FLUENT 13.0 using a 2D axis symmetric swirl model which introduces a velocity vector in the third dimension. This model assumes rotational symmetry and thereby neglecting angular differences. The equation that solves the swirl velocity can be stated as

$$\frac{\partial}{\partial t}(\rho w) + \frac{1}{r}\frac{\partial}{\partial x}(r\rho uw) + \frac{1}{r}\frac{\partial}{\partial r}(r\rho uw) = \frac{1}{r}\frac{\partial}{\partial x}\left[r\mu\frac{\partial w}{\partial x}\right] + \frac{1}{r^2}\frac{\partial}{\partial r}\left[r^3\mu\frac{\partial}{\partial r}\left(\frac{w}{r}\right)\right] - \rho\frac{vw}{r} \qquad (6.1.1)$$

where w is the swirl velocity, u is the axial velocity, v is the radial velocity, r and x is the radial and axial coordinate respectively.

To enable a two dimensional geometry a disk impeller is used instead of a blade impeller. The mesh is shown in figure 6.1.1 and general information of the domain dimensions and size are present in table 5.1.1.

Table 6.1.1 Domain dimentions.

Description	Value
Radius	142.5 mm
Hight	168.1 mm
Disk hight	6.9 mm
Number of cells	70332
Smallest cell volume	3.88e-10 m^3
Largest cell volume	1.42e-6 m^3

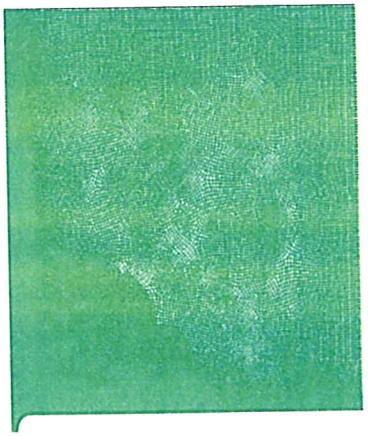

Figure 6.1.1 Mesh of the domain.

6.2 Initial conditions

The simulation is performed based on a converged flow field that represents the flow conditions after the dry mixing period. The system consists of air and microcrystalline cellulose as a granular phase using a laminar Euler-Euler model, turbulence are not expected to have a big influence on the dense particle system why it is excluded from the model. Table 6.2.1 presents data that have been used in the simulations.

Table 6.2.1 Particle and gas properties.

Parameter	Description	Value
ρ_g	Gas density	1.225 kg/m^3
μ_g	Gas viscosity	1.7894e-05 Pas
d_0	Particle diameter	50 µm
ρ_s	Solid density	740 kg/m^3
e	Coefficient of restitution	0.9
$\alpha_{s,min}$	Kick-in volume fraction for frictional stress	0.5
$\alpha_{s,max}$	Maximum particle packing	0.63
φ	Angle of internal friction	28°
Fr	Model constant	0.05
n	Model constant	2
p	Model constant	3

Six and four moments have been modeled for the population balance. The moments are initialized based on the total solid volume which can be directly used for the third moment. Assuming the granular phase is homogenous all other moments can be estimated from the third moment and the initial particle diameter as

$$m_0 = \frac{V_{s,cell}}{d_0^3 K_v} \tag{6.2.1}$$

$$m_1 = \frac{V_{s,cell}}{d_0^2 K_v} \tag{6.2.2}$$

$$m_2 = \frac{V_{s,cell}}{d_0 K_v} \tag{6.2.3}$$

$$m_3 = \frac{V_{s,cell}}{K_v} \tag{6.2.4}$$

$$m_4 = \frac{d_0 V_{s,cell}}{K_v} \tag{6.2.5}$$

$$m_5 = \frac{d_0^2 V_{s,cell}}{K_v} \tag{6.2.6}$$

6.3 Boundary conditions

The granulator is modeled as a closed container and all boundaries are thus walls where no slip condition is applied for both phases. For the granular phase this is not a totally reliable physical description but it is used to enhance high shear forces in the granular bed.

The bottom plate is set to a rotation speed of 312 rounds per minute. To ease the swirl velocity calculation, this is done by letting the disk itself be stationary and all cells together with the coordinates rotates relative the plate and with the walls stationary in relation to the cells.

6.4 Aggregation efficiency models

The particle aggregation efficiency is based on the amount liquid binder available. Two different expressions have been used and are described below.

6.4.1 Liquid saturation model

The first efficiency expression is based on the level of liquid saturation, S, which was successfully used by Darelius et al. (2005) and is defined as the liquid volume in a granule over the porous volume. The liquid saturation and the aggregation efficiency can be expressed as

$$S = H\frac{(1-\varepsilon)}{\varepsilon}\frac{\rho_s}{\rho_l} \tag{6.4.1}$$

$$\psi_1 = S/S_{max} \tag{6.4.2}$$

where H is the liquid to solid ratio [g/g] and ε is the granule porosity. S_{max} is redefined as an over saturated granule with pores filled with liquid and with a liquid film covering the granule surface. In the originall model for the aggregation efficiency, S_{max} was the maximum obtained liquid saturation for each experiment in Darelius et al. (2005).

6.4.2 Accessible binder fraction model

This physical model was used in Rajniak et al. (2009) where the accessible binder fraction is assumed to be locally distributed the same for all particles. The geometricall part is then divided in probabilities for a wet-wet, wet-dry or a dry-dry collision.

$$\psi_{wet+wet}^{geom} = \eta^2 \tag{6.4.3}$$

$$\psi_{wet+dry}^{geom} = 2\eta(1-\eta) \tag{6.4.4}$$

$$\psi_{dry+dry}^{geom} = (1-\eta)^2 \tag{6.4.5}$$

The accessible binder liquid and the binder liquid thickness can be estimated from simulations performed by Stepanek et al. (2009) as

$$\eta = \frac{1}{1+e^{-b(x-c)}} \tag{6.4.6}$$

$$\lambda = de^{f(x-g)/3} \tag{6.4.7}$$

where all data fitted parameters is present in table 6.4.1. A modified physical criterion can be used stated as in Rajniak et al. (2009):

$$\psi_{wet+wet}^{phys} = \begin{cases} 1 \; if \; St_v \leq 2ln\frac{\lambda}{h_a} \\ 0 \; if \; St_v > 2ln\frac{\lambda}{h_a} \end{cases} \tag{6.4.8}$$

$$\psi_{wet+dry}^{phys} = \begin{cases} 1 \; if \; St_v \leq 2ln\frac{\lambda}{2h_a} \\ 0 \; if \; St_v > 2ln\frac{\lambda}{2h_a} \end{cases} \tag{6.4.9}$$

The final expression for the total agglomeration efficiency can be expressed as

$$\psi_2 = \psi_{wet+wet}^{geom}\psi_{wet+wet}^{phys} + \psi_{wet+dry}^{geom}\psi_{wet+dry}^{phys} \tag{6.4.10}$$

Table 6.4.1 Particle shape descriptors and data fitted parameters for aggregation efficiency (Rajniak et al., 2009).

Parameter	a	b	c	f	g	L	ha [µm]
Value	0.211	35.1	0.129	25.9	0.327	0.62	6.3

6.5 Binder liquid

Water is used as binder liquid, the concentration H [kg liquid/kg solid] is modeled through a transport equation, the binder liquid properties that has been used is present in table 6.4.1. Because the liquid is expected to attach to the particle surfaces it is totally governed by the granular phase. Also, the liquid is expected to follow the granules and thus no diffusion term is present.

$$\frac{\partial}{\partial t}(\alpha_s \rho_s H) + \nabla \cdot (\alpha_s \rho_s \vec{u}_s H) = S_H \tag{6.5.1}$$

Table 6.5.1 Properties of binder liquid.

Parameter	Description	Value
ρ_l	Binder density	1000 kg/m^3
μ_l	Binder viscosity	0.001 Pas

6.5.1 Spray model

The liquid binder spray is modeled by tracking the granular bed surface. This is done by sorting the cell volumes within a specified granular volume fraction range and cutting off the sections close to the disc and the wall (figure 6.5.1). At the surface, the liquid binder transport equation is modified through the source term which adds moisture based on a specified total amount of liquid binder and total spray time. Spray specifications are presented in table 6.4.2.

$$S_H = \frac{H_{tot}}{m_s V_{surf} t} \tag{6.5.2}$$

Table 6.5.2 Spray specifications.

Parameter	Description	Value
H_{tot}	Total liquid binder amount	0.6 g/g
t	Spray time	30 s
$\alpha_{s,min}$	Max volume fraction for surface tracking	0.40
$\alpha_{s,max}$	Min volume fraction for surface tracking	0.15
r_{min}	Min radius for surface tracking	20 mm
h_{max}	Max height for surface tracking	123 mm

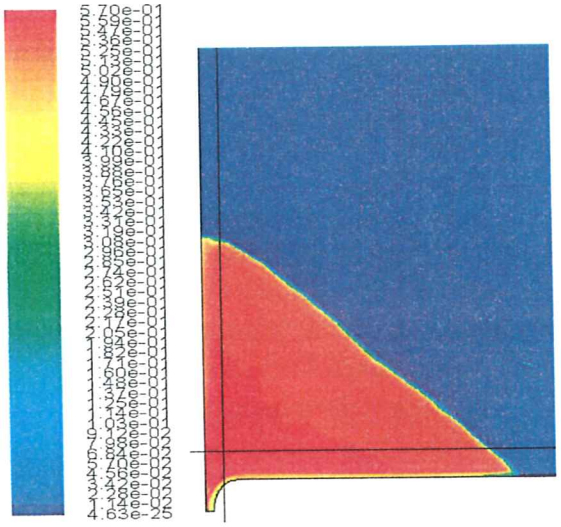

Figure 6.5.1 Spray zone area.

6.6 Simulations

Different initializations of moments are evaluated. The different initialization setups are listed in table 6.6.1 with an initial diameter of 50μm. Both a four moment model and a six moment model are evaluated.

Table 6.6.1 Moment initialization, m0 – m5 are set according to equations 6.2.1 -6.2.6.

Moment	Init 1	Init 2	Init 3	Init 4
0	m_0	m_0	m_0	m_0
1	m_1	m_1	m_1	m_1
2	m_2	0	m_2	0
3	m_3	0	m_3	0
4	-	-	m_4	0
5	-	-	m_5	0

Five different variations of the aggregation kernel are simulated and are listed in table 6.6.2. Simulation are performed without updating the flow field which implies that the flow field is considered as steady state as it affects the population balance and the binder liquid transport. The population balance equation and the binder liquid equation are simulated with a timestep of 0.001s. The porosity and aggregation rate constant are set to 0.4 and 1e-4 respectively.

Table 6.6.2 Combinations of the aggregation kernel simulated.

Collision model	Efficiency expression
EKE	ψ_1
EKE	ψ_2
KTGF	ψ_1
KTGF	ψ_2
KTGF	ψ_2^{geom} $(\psi_2^{phys} = 1)$

7 Results and discussion

In this chapter results from the simulations are presented together with a discussion of the observations of the model.

7.1 Flow field

The granular phase velocity field is composed of a rotating flow pattern which is shown in figure 7.1.1. The length of the arrows corresponds to the relative velocity in the axial radial plane. The large arrows at the surface mean that particles have relatively high radial and axial velocities that are dominating over the swirl velocity. The smaller arrows in the middle indicate that it is almost no movement in the axial radial plane but a dominating swirl velocity component. The highest velocity magnitudes are found at the bottom because of the no slip condition against the rotating disc.

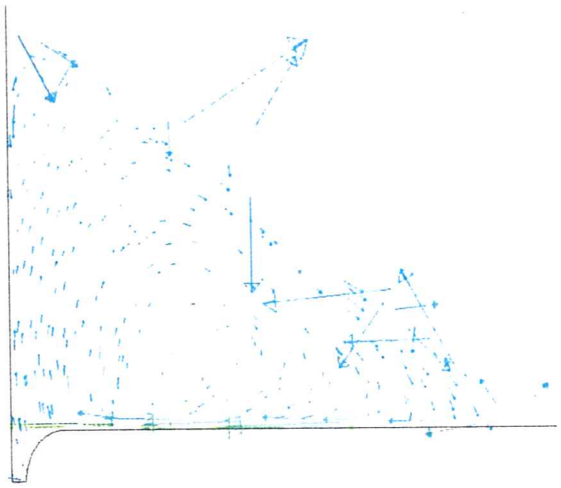

Figure 7.1.1 Velocity vectors of the granular phase (d_s = 50μm) in axial and radial direction, colored by velocity magnitude.

7.2 Number density function

Simulations were performed with four and six moments, figure 7.2.1 shows the initial number distribution function for the different cases.

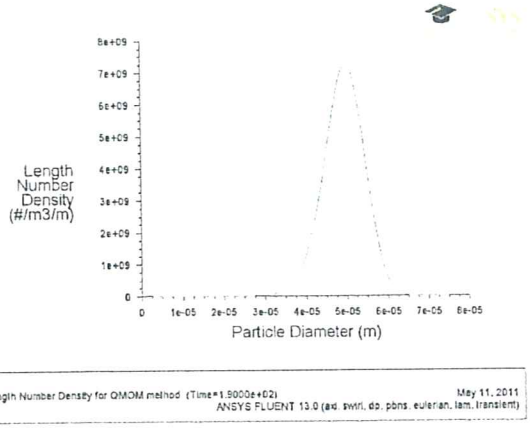

(a)

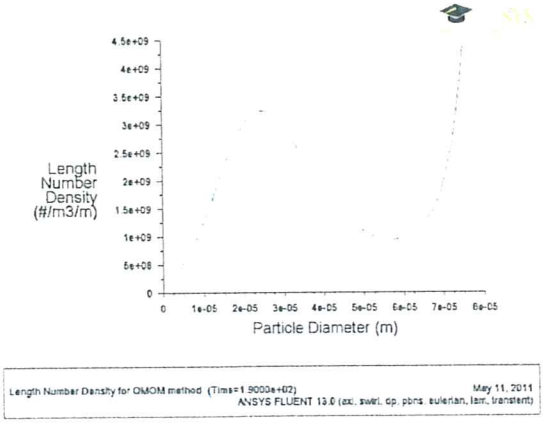

(b)

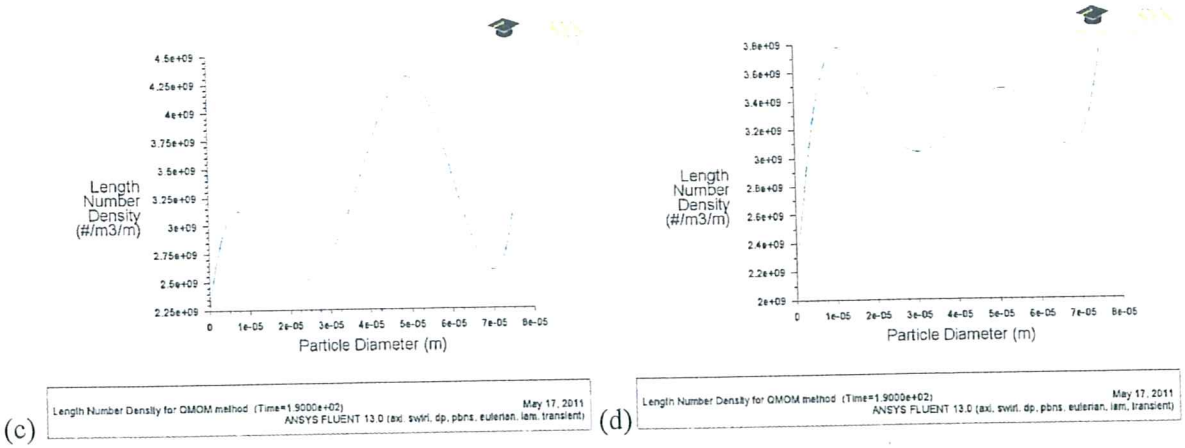

Figure 7.2.1 Initial number density function for the cases: a) Four moments model with all four moments initialized. b) Four moments model with two first moments initialized and moment 3 and 4 were set to zero. c) Six moments model with all moments initialized. d) Six moments model with two first moments initialized and all other moments set to zero.

The two distributions where only two moments were initialized according to equation 6.2.1 and 6.2.2 (figure7.2.1 b and d) indicate that the reconstruction of the distributions are still affected by the presence of the other moments in the model since the two initialized moments only holds enough information to describe a Gaussian distribution. Only when four moments were used, initialized according to equation 6.2.1-6.2.4, a distribution close to a Gaussian distribution was obtained. All further results are based on this choice of moment initialization. It is also observed that the four moments models results in bimodal distributions while six moments models results in trimodal distributions (initial distribution in figure 7.2.1a have a small fraction close to the origin).

All simulations show similar development of the number distribution function. The initial distribution is typically divided in two parts. The evolution of the particle distribution results in the peak at 20μm (figure 7.2.2) which decreases in time, this implies that less particles of this size are present in the system as time elapses. The formation of this peak is unphysical since the population balance includes aggregation only (compare to the initial distribution, figure 7.2.1a). The peak at the right boundary typically gets steeper with time rather than move along the axis. It seems that a maximum particle size prevents the particle distribution development.

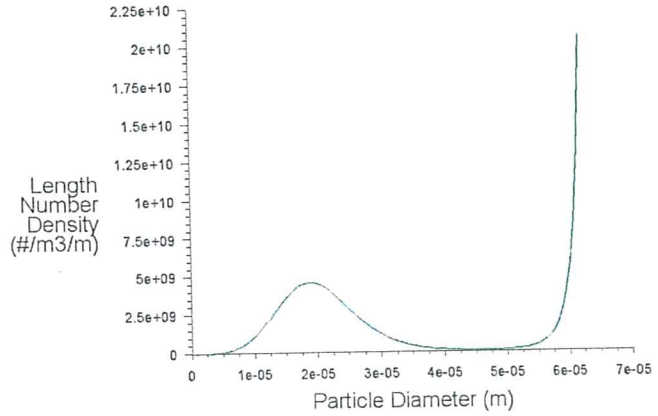

Figure 7.2.2 Number density function after 15s using KTGF based collision model and binder liquid saturation efficiency model.

7.3 Spray and binder liquid mixing

Figure 7.3.1 shows the spray zone and the liquid mixing development the first 40s. Since the moisture is not modeled as an eulerian phase it will not affect the flow field through the momentum equations. The liquid does not occupy any volume of the domain why this approach is best suited only if a low liquid fraction is expected.

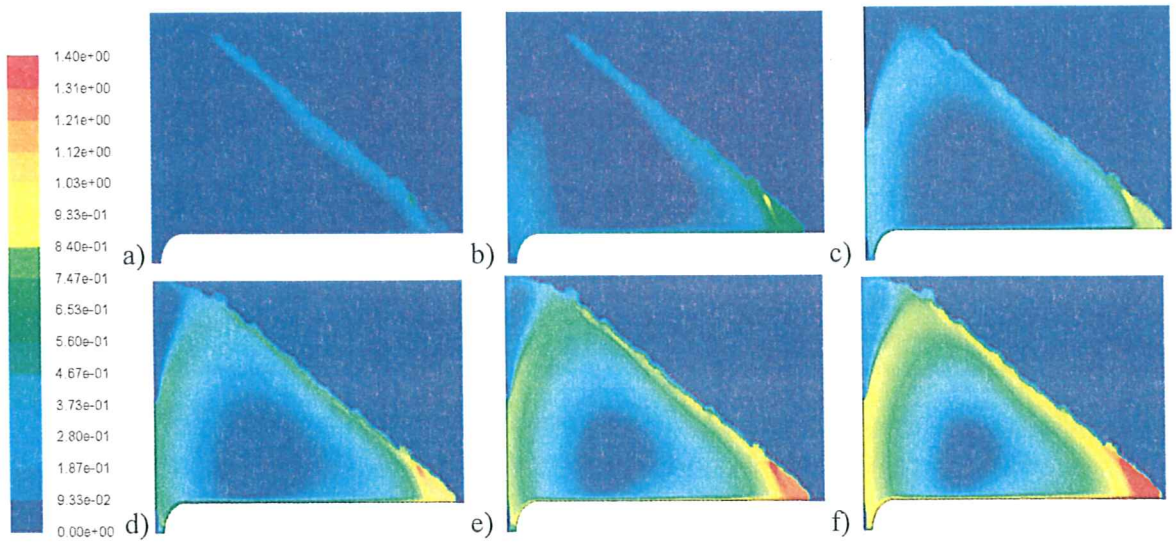

Figure 7.3.1 Binder liquid distribution after a) 1s b) 5s c) 10s d) 20s e) 30s f) 40s.

A significant loss of binder liquid is obtained (figure 7.3.2) which most likely is due to numerical or code errors. The surface of the granular bed consists of a very sharp gradient of the volume fractions, because of this the volume fraction limits for surface tracking have to be narrow. This means that the binder liquid spray zone consists of a relatively small number of cells where the liquid binder is added. This leads to large gradients of binder liquid which could be one source of numerical difficulties. However, this error does not vary between simulation cases since the same flow field is used and the same numerical scheme is used for the binder liquid transport equation. The spray time increases with about 10s due to binder liquid mass imbalance during the simulations. The binder liquid is only used for qualitative analysis of the aggregation kernels why this spray model is still considered sufficient.

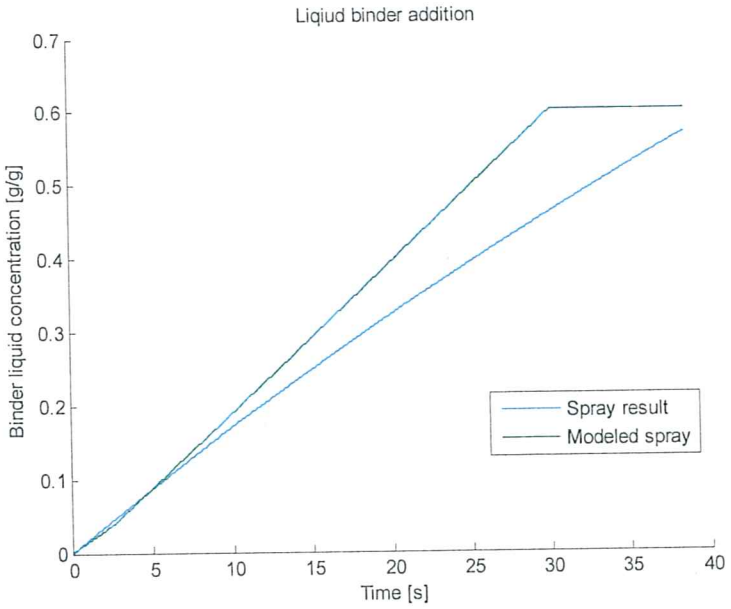

Figure 7.3.2 Comparison between modeled spray and observed liquid addition.

7.4 Aggregation kernels

There exists three different aggregation kernels integrated in ANSYS FLUENTs population balance module. However, none of them were appropriate in this work.

At first, there is the Brownian motion kernel which is based on collisions due to random movement, this model is best suited if particles are very small.

The second available aggregation kernel is derived by Luo (1993). This is a general kernel stated as a product of collision frequency and aggregation probability where the probability as well as the collision frequency depends on the turbulent mixing. However, the granular system is very dense and will not be affected by the gas phase in the particle bed. Due to the generally low velocities in the system and high weight of the particles there will be no need of a turbulence model describing the flow field and the kernel is thus not applicable.

The third model is the turbulent aggregation kernel that divides the collision rate mechanisms in two categories: A viscous subrange and an inertial subrange. The different models are based on empirical relations and are applied dependent on the ratio of the particle size and the Kolmogorov microscale. This model is also inapplicable since a turbulence model is required.

7.4.1 Aggregation efficiency

Comparing the binder liquid distribution for the two different aggregation expressions it is observed that the accessible binder fraction model is more sensitive to binder liquid. The binder liquid distribution for the liquid saturation model is shown in figure 7.4.1. The system contains 0.57g binder liquid/g solid after 38s.

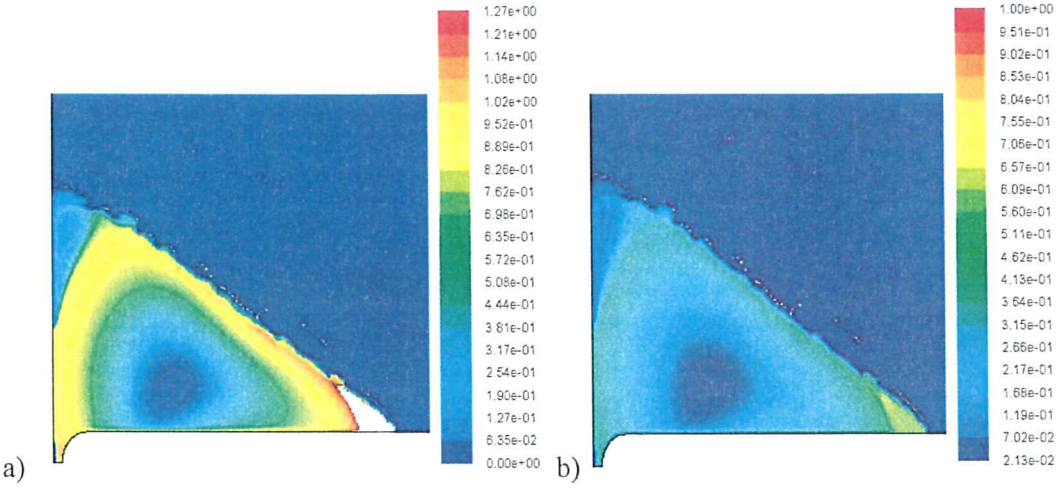

Figure 7.4.1 a) Contours of binder liquid distribution. b) Contours of aggregation efficiency.

The aggregation efficiency for the accessible binder fraction model (figure 7.4.2) shows a higher efficiency distribution even though there is less binder liquid in the system (H_{tot} = 0.22 g/g, t = 13.1s).

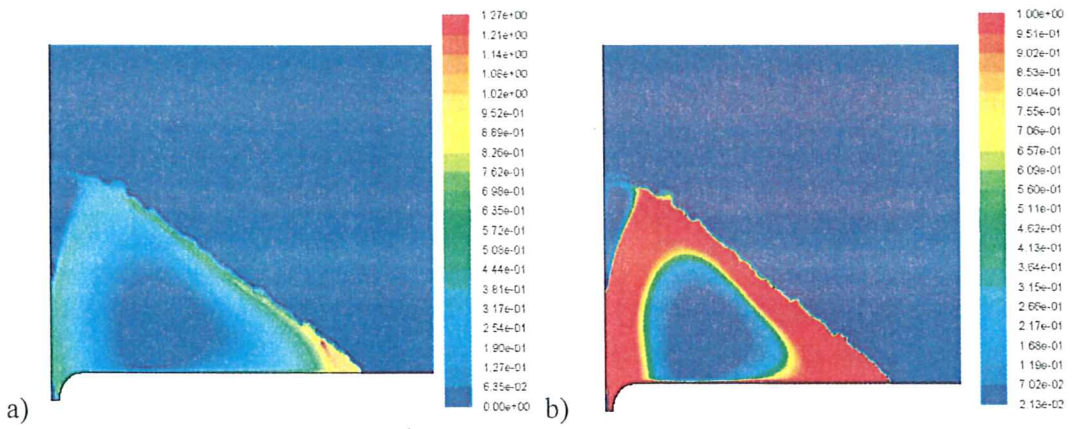

Figure 7.4.2 a) Contours of binder liquid distribution. b) Contours of aggregation efficiency.

Figure 7.4.3 shows how the efficiency is proportional to the binder liquid amount for the liquid saturation model. The accessible binder fraction model gives lower efficiency at lower binder liquid concentrations but increases faster and reaches full efficiency at a binder liquid concentration of about 0.4 g/g. A major explanation of the differences between the two models is that the accessible binder fraction model is physical while the saturation model only contains information that is crucial for the physics but there is no physical relation saying that the level of liquid saturation corresponds to the aggregation efficiency. The proportionality can according to the model be adjusted through two estimated parameters, the porosity and the definition of the maximum liquid saturation which gives fully efficient aggregation.

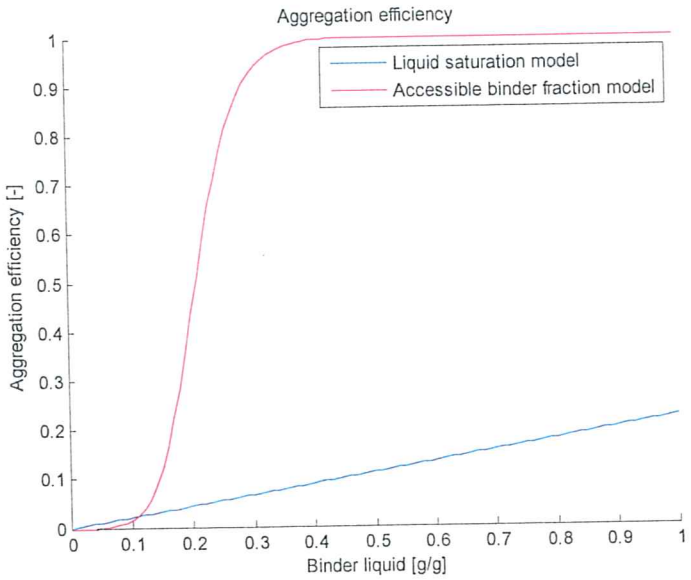

Figure 7.4.3 Aggregation efficiency models binder liquid dependency.

7.4.2 Collision frequency

The KTGF based collision frequency model is used trying to extract information about the granular temperature dependence from the collision rate constant. Figure 7.4.4 shows that the granular temperature in the system is very low in the particle bed (< 1e-6 m^2/s^2) except at the surface and close to the disk impeller. According to equation 5.3.5 the collision frequency is proprtional to the square of the granular temperature which increases the aggregation rate in the higher granular temperature regions. However, the aggregation is expected to be favored in regions where the momentum exchange between particles is high and in such a dense system the frictional part of the momentum transfer is expected to be dominating. If the major part of the momentum transfer is due to friction then the granular temperature should not have a big influence on the aggregation rate and consequently the KTGF based model is not necessarily more accurate in dense particle systems.

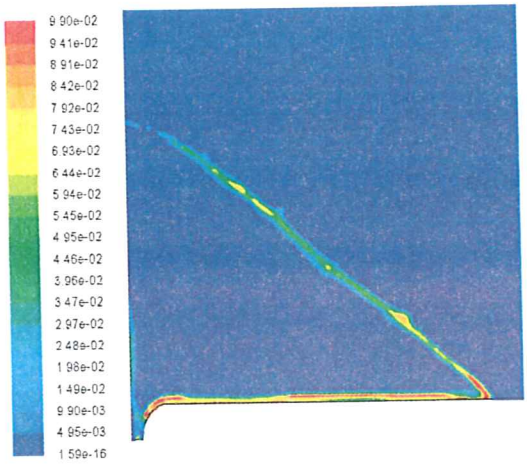

Figure 7.4.4 Granular temperature profile in the particle bed.

7.5 Moment evolution

For the different model setups the changes in population and volume are followed, also the Sauter mean diameter is evaluated.

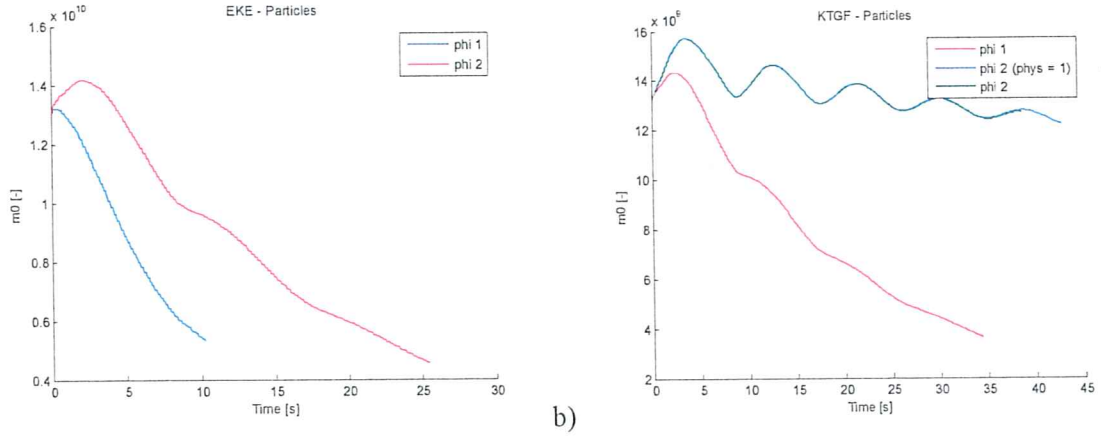

a) b)

Figure 7.5.1 The zero moment representing the total number of particles in the system for the a) EKE-kernel and b) the KTGF-based kernel

From figure 7.5.1a it is observed that the number of particles and thus the total granular phase volume as well are increasing in the first seconds. One possible explanation for this phenomenon would be that it is a cause of an unphysical initialization of the moments which does not relate to each other correctly. Since the initial number distribution function are Gaussian (figure 7.2.1a) the relation of the total volume to total area, total length and number of particles are unknown and the initial moments are thus only approximations. The impact of the physical criterion in the KTGF-based efficiency seems negligible in this system (figure 7.5.1b). This is caused by the low granular temperature in the system which provides generally low collision velocities and thus small viscous Stokes number which results in a physical part that almost always equals one.

The variations of the third moment are obviously the same for all cases (figure 7.5.2). As for the particle amount a wave function is observed which cause is not obvious. Further simulation would answer whether the moment (total moment in the domain) would converge close to its physical value.

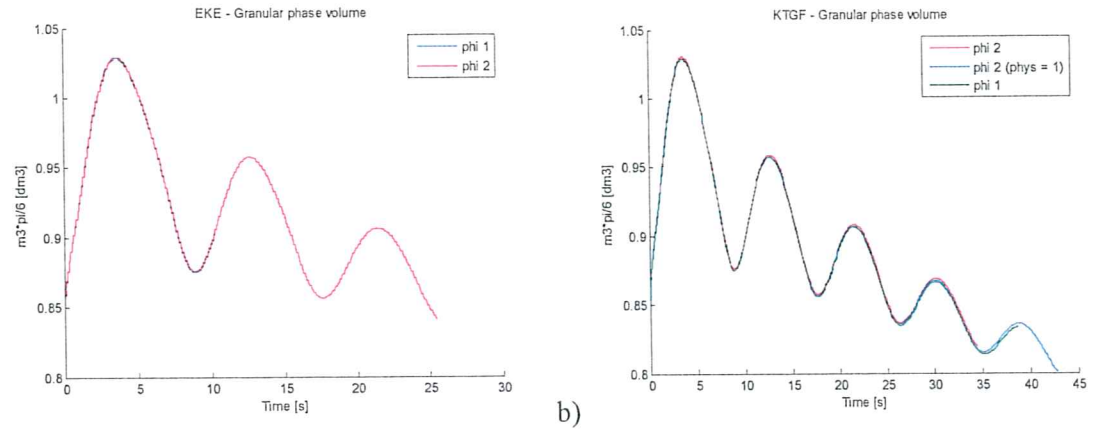

a) b)

Figure 7.5.2 The third moment representing the total granular phase volume for the a) EKE-kernel and b) the KTGF-based kernel.

The Sauter mean diameter does not show any differences between the two frequency expressions (figure 7.5.3). For the EKE-kernel it is observed that the efficiency based on liquid saturation favors the aggregation process at the simulated process conditions.

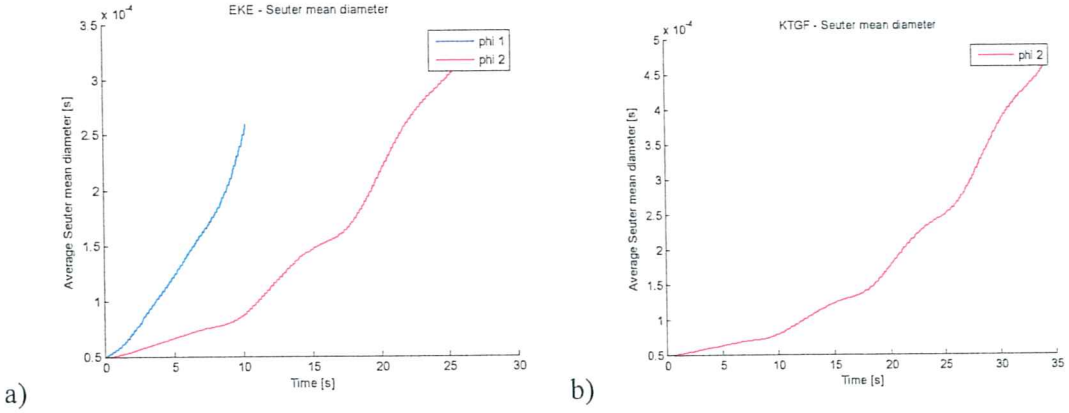

a) b)

Figure 7.5.3 The Sauter mean diameter for the a) EKE-kernel and b) the KTGF-based kernel.

8 Conclusions

The ANSYS FLUENT software offer several possible kernels for both aggregations a breakage. However, they are limited to turbulent flows except for the Brownian motion kernel.

The theory and implementation of the population balance equation using the QMOM has been reported promising in the literature. In this work several parts of the solver stands unclear. For better understanding of the number distribution function improved understanding of the reconstruction of its moments is crucial. The development of moments does not correctly correspond to their physical meaning which cause is uncertain but can be due to source code errors.

The binder liquid can successfully be modeled as proposed for qualitative purposes as long as the exact amount binder liquid is not needed.

In dense systems, the granular temperature is of minor importance concerning the collision frequency. The granular temperature does not have a big influence on the aggregation efficiency unless higher velocities are present in the system.

References

Abberger T., Population Balance Modelling of Granulation, Handbook of Powder Technology vol. 11 2007, 1109-1186.

Anderson T. B., Jackson R., A fluid mechanical description of fluidizied beds. Industrial & Engineering Chemistry Fundamentals 1967, 6, 527-593.

Andersson B, Andersson R, Håkansson L, Mortensson M, Sudiyo R, Wachem B., Computational fluid dynamics for chemical engineers. 6th Edition, Chalmers University of Technology 2010.

Darelius A., Rasmuson A., Niklasson Björn I., Folestad S., High shear wet granulation modeling – a mechanistic approach using population balances, Powder Technaology 2005 160:209-218.

Ding J, Gidaspow D., Bubbling fluidization model using kinetic theory of granular flow, AlChE Journal 1990 6:523-538.

Ennis B. J., Tardos G., Peffer R., A microbased characterization of granulation phenomena, Powder Technology 1991 65:257-272.

Gidaspow D., Multiphase flow and fluidization – Continuum and kinetic theory descriptions, Academic Press 1994, London, England.

Goldschmidt M. J. V., Hydrodynamic Modelling of Fluidizied Bed Granulation, PhD Thesis, Twente University, 2001.

Gordon R. G., Error Bounds in Equilibrium Statistical Mechanics, Journal of Mathematical Physics 1968 56:655–633.

Hounslow M. J., The Population Balance as a Tool for Understanding Particle Rate Processes, Kona 1998 179-193.

Hounslow M. J, Ryall R. L, Marshall V. R. A Discretized Population Balance for Nucleation, Growth, and Aggregation 1988 AIChE Journal. 34(11):1821–1832.

Hulburt H., Katz S., Some Problems in Particle Technology. A Statistical Mechanical Formulation 1964 19:555.

Johnson P. C, Jackson R. Frictional collisional constitutive relations for antigranulocytes-materials, with application to plane shearing, Journal of Fluid Mechanics 1987 176:67-93.

Liu L. X., Litster J. D., Iveson S. M., Ennis B. J., Coalescence of deformable granules in wet granulation processes, AlChE Journal 2000 46:529-539.

Liu L. X., Litster J. D., Population balance modeling of granulation with a physically based coalescence kernel, Chemical Engineering Science 2002 57:2183-2191.

Lun C. K. K, Savage S. B, Jeffrey D. J, Chepurniy N., Kinetic theories for granular flow: inelastic particles in couette flow and slightly inelastic particles in a general flow field, Journal of Fluid Mechanics 1984 140:223-256.

Luo H., Coalescence, Breakup and Liquid Circulation in Bubble Column Reactors, PhD thesis from the Norwegian Institute of Technology. Trondheim, Norway, 1993.

Marchisio D. L., Pikturna J. T., Fox R. O. Virgil R. D., Quadrature Method of Moments for Population-Balance Equations 2003(a) AIChE Journal 49:1266-1276.

Marchisio D. L., Virgil R. D., Fox R. O. Quadrature Method of Moments for Aggregation-Breakage Processes, Journal of Colloid and Interface Science 2003(b) 258:322–334.

McGraw R., Description of Aerosol Dynamics by the Quadrature Method of Moments, Aerosol Science and Technology 1997 27: 255–265.

Rajniak P., Stpanek F., Dhanasekharan K., Fan R., Chern R. T., A combined experimental and copmputational study of wet granulation in a Wurster fluid bed granulator, Powder Technology 2009 189:190-201.

Ramkrishna D., Population Balances, Academic Press, London, 2000.

Scarlett B., Particle Populations – to balance or not to balance, that is the question! Powder Technology 2001. 125, 1-4.

Schaeffer D. G., Instability in the evolution equations describing incompressible granular flow, Journal of Differential Equations 1987 66:19-50.

Stepanek F., Rajniak P., Mancinelli C., Ramachandran R., Distribution and accessibility of binder liquid in wet granules, Powder Technology 2009 189:376-384.

Syamlal M, Rogers W, O'Brien T. J., MFIX Documentation: Volume1, Theory Guide. National Technical Information Service, Springfield, VA. DOE/METC-9411004, NTIS/DE9400087 1993.

Wen C. Y, Yu Y. H., Mechanics of fluidization. Chemical Engineering Progress Symposium Series 1966 62:100-111.